

Supplement of Atmos. Chem. Phys., 20, 2445–2470, 2020
<https://doi.org/10.5194/acp-20-2445-2020-supplement>
© Author(s) 2020. This work is distributed under
the Creative Commons Attribution 4.0 License.



Supplement of

Amplification of black carbon light absorption induced by atmospheric aging: temporal variation at seasonal and diel scales in urban Guangzhou

Jia Yin Sun et al.

Correspondence to: Cheng Wu (wucheng.vip@foxmail.com), Dui Wu (wudui.vip@foxmail.com),
and Zhen Zhou (zhouzhen@gig.ac.cn)

The copyright of individual parts of the supplement might differ from the CC BY 4.0 License.

Back trajectory and wind rose analysis

Back trajectories analysis showed that in wet season most air masses were from South China Sea, with only 31.67% air masses were locally influenced (Figure S15a). Among the 3 back trajectory clusters in wet season, the locally influenced air masses exhibit the shortest back trajectory (C1), leading to the highest EC concentration ($2.01 \pm 1.22 \mu\text{gC m}^{-3}$). As the back trajectory distance increased from C2 to C3, the corresponding EC decreased from 2.01 ± 0.88 to $1.56 \pm 0.67 \mu\text{gC m}^{-3}$. During dry season, air masses were dominated by those of northern origin. EC concentrations also exhibit gradient on the trajectory path length. Long-path (C3) trajectories lead to low EC concentrations ($2.01 \pm 1.46 \mu\text{gC m}^{-3}$), while short-path trajectories lead to higher concentrations (C1: $3.50 \pm 2.13 \mu\text{gC m}^{-3}$; C2: $2.52 \pm 1.91 \mu\text{gC m}^{-3}$).

The dependence of MAE_{520} on wind speed and wind direction was investigated in Figure S16, which is generated using ZeFir (Petit et al., 2017). In wet season, the southeast wind dominates (Figure S16b), which is in consistency with back-trajectory analysis discussed above. MAE_{520} did not show obvious dependence on wind speed and wind direction in the wet season (Figure S7a). In dry season, the northwestern wind prevailed (Figure S16d). High MAE_{520} was spotted from west with a wind speed at 7 m s^{-1} (Figure S16c), suggesting regional transport of aged air masses.

Dependence of $E_{\text{abs}520}$ on air masses was investigated by back-trajectory cluster analysis as shown in Figure S15. In wet season, the highest $E_{\text{abs}520}$ (1.71 ± 0.58) was found from the shortest back trajectories (C1), suggesting the local episodic events. The high $E_{\text{abs}520}$ from C1 (northeasterly air mass) was also confirmed by the wind rose plot (Figure S17). The elevated $E_{\text{abs}520}$ of C1 was likely associated with high SOC/OC ratios from Aug 18 to 23 as shown by the time series plot in Figure S4a. The two oceanic air mass clusters (C2 and C3) exhibit deviated $E_{\text{abs}520}$ characteristics. C3 represents more aged oceanic air masses as evidenced by the lower EC (1.56 ± 0.67) and higher $E_{\text{abs}520}$ (1.58 ± 0.57). In contrast, C2 has relatively lower $E_{\text{abs}520}$ (1.40 ± 0.38) but higher EC. In dry season, $E_{\text{abs}520}$ did not show clear dependence on back trajectory clusters as the $E_{\text{abs}520}$ falls into a narrow range (1.24-1.34) between C1-C3. E_{abs} dependence on wind speed and wind direction was examined in Figure S17. $E_{\text{abs}520}$ showed little dependence on wind speed and the high E_{abs} occurrences (Figure S17) was largely overlapped with the high MAE as shown in Figure S16.

References

- Drinovec, L., Močnik, G., Zotter, P., Prévôt, A. S. H., Ruckstuhl, C., Coz, E., Rupakheti, M., Sciare, J., Müller, T., Wiedensohler, A., and Hansen, A. D. A.: The "dual-spot" Aethalometer: an improved measurement of aerosol black carbon with real-time loading compensation, *Atmos. Meas. Tech.*, 8, 1965-1979, doi: 10.5194/amt-8-1965-2015, 2015.
- Petit, J. E., Favez, O., Albinet, A., and Canonaco, F.: A user-friendly tool for comprehensive evaluation of the geographical origins of atmospheric pollution: Wind and trajectory analyses, *Environ Modell Softw*, 88, 183-187, doi: 10.1016/j.envsoft.2016.11.022, 2017.

Table S1. MAE values from study by Drinovec et al. (2015) was adopted for $\sigma_{\text{abs_total}}$ back-calculations at different wavelengths

| Wavelength (nm) | MAE (m^2g^{-1}) |
|-----------------|-----------------------------------|
| 370 | 18.47 |
| 470 | 14.54 |
| 520 | 13.14 |
| 590 | 11.58 |
| 660 | 10.35 |
| 880 | 7.77 |
| 950 | 7.19 |

Table S2. Grouping criteria of EC-containing particles data from SPAMS used in this study. EC-containing particles were defined by the criteria shown below. Then EC-containing particles were further grouped into two categories, EC-fresh and EC-aged. EC-aged particles were extracted from EC-containing particles using the ion markers with the RPA thresholds listed below. The remaining EC-containing particles were defined as EC-fresh particles.

| Species | m/z | Marker Ion | Peak Area | Relative Peak Area | Function |
|---------------|--------------------------------|--|-----------|--------------------|----------|
| EC-containing | 12 | [C] ⁺ | >50 | >0.005 | or |
| | 24 | [C ₂] ⁺ | >50 | >0.005 | or |
| | 36 | [C ₃] ⁺ | >50 | >0.005 | or |
| | 48 | [C ₄] ⁺ | >50 | >0.005 | or |
| | 60 | [C ₅] ⁺ | >50 | >0.005 | or |
| | -12 | [C] ⁻ | >50 | >0.005 | or |
| | -24 | [C ₂] ⁻ | >50 | >0.005 | or |
| | -36 | [C ₃] ⁻ | >50 | >0.005 | or |
| | -48 | [C ₄] ⁻ | >50 | >0.005 | or |
| -60 | [C ₅] ⁻ | >50 | >0.005 | or | |
| EC-aged | 27 | [C ₂ H ₃] ⁺ | >50 | >0.005 | or |
| | 37 | [C ₃ H] ⁺ | >50 | >0.005 | or |
| | 43 | [C ₂ H ₃ O] ⁺ | >50 | >0.005 | or |
| | -46 | [NO ₂] ⁻ | >100 | >0.05 | or |
| | -62 | [NO ₃] ⁻ | >100 | >0.05 | or |
| | -97 | [HSO ₄] ⁻ | >100 | >0.05 | or |

Table S3. SPAMS measurement statistics in this study.

| Season | Single particle classes | number count | number fraction |
|------------|-------------------------|--------------|-----------------|
| Wet season | mass particles | 327453 | 100% |
| | EC-containing | 120351 | 36.75% |
| | EC-fresh | 10919 | 3.33% |
| | EC-aged | 109432 | 33.42% |
| Dry season | mass particles | 2212688 | 100% |
| | EC-containing | 595180 | 26.90% |
| | EC-fresh | 55940 | 2.53% |
| | EC-aged | 539240 | 24.37% |

Table S4. Spectral optical properties of BC between wet and dry seasons.

| wavelength (nm) | | 370 | 470 | 520 | 590 | 660 | 880 | 950 |
|---|-----------------|--------|--------|--------|--------|--------|--------|--------|
| MAE_p (m² g⁻¹) | wet season | 14.2 | 10.2 | 8.6 | 7.46 | 6.36 | 4.51 | 4.3 |
| | dry season | 28.7 | 20.1 | 16.8 | 14.4 | 12.3 | 8.61 | 8.18 |
| E_{abs} | wet season mean | 1.55 | 1.51 | 1.51 | 1.51 | 1.51 | 1.51 | 1.50 |
| | wet season S.D. | 0.53 | 0.51 | 0.50 | 0.50 | 0.50 | 0.49 | 0.49 |
| | dry season mean | 1.35 | 1.29 | 1.29 | 1.24 | 1.29 | 1.29 | 1.29 |
| | dry season S.D. | 0.34 | 0.29 | 0.28 | 0.19 | 0.27 | 0.27 | 0.27 |
| σ_{abs} (Mm⁻¹) | wet season mean | 39.18 | 27.90 | 23.62 | 20.44 | 17.39 | 12.25 | 11.64 |
| | wet season S.D. | 18.98 | 13.42 | 11.27 | 9.74 | 8.28 | 5.87 | 5.59 |
| | dry season mean | 95.38 | 65.35 | 54.56 | 37.61 | 39.67 | 27.55 | 26.14 |
| | dry season S.D. | 62.02 | 42.74 | 35.71 | 33.05 | 26.08 | 18.26 | 17.36 |
| k | wet season mean | 0.0072 | 0.0076 | 0.0078 | 0.0081 | 0.0081 | 0.0075 | 0.0074 |
| | wet season S.D. | 0.0004 | 0.0005 | 0.0006 | 0.0007 | 0.0009 | 0.0016 | 0.0018 |
| | dry season mean | 0.0066 | 0.0072 | 0.0072 | 0.0075 | 0.0072 | 0.0072 | 0.0072 |
| | dry season S.D. | 0.0013 | 0.0018 | 0.0018 | 0.0020 | 0.0037 | 0.0037 | 0.0039 |

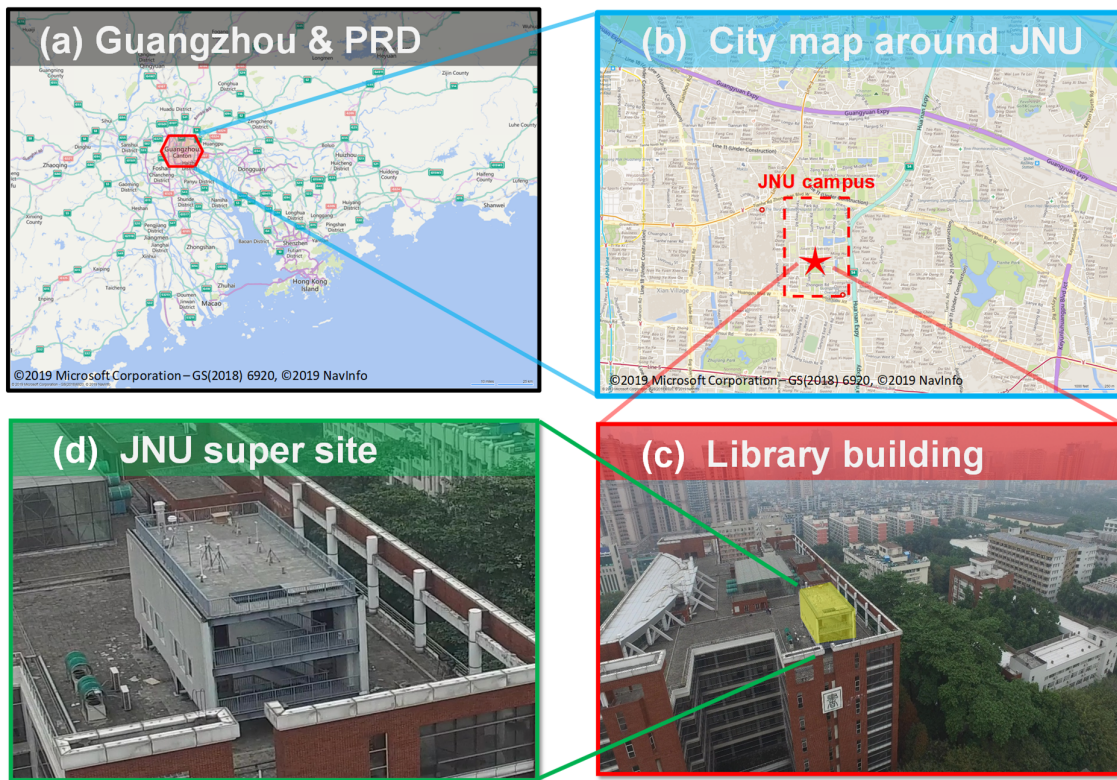


Figure S1. Location of the sampling site. (a) Map of PRD region. (b) City map around JNU. The dash line in red indicates the area of JNU campus in the downtown of Guangzhou. (c) The JNU library building. (d) JNU super site

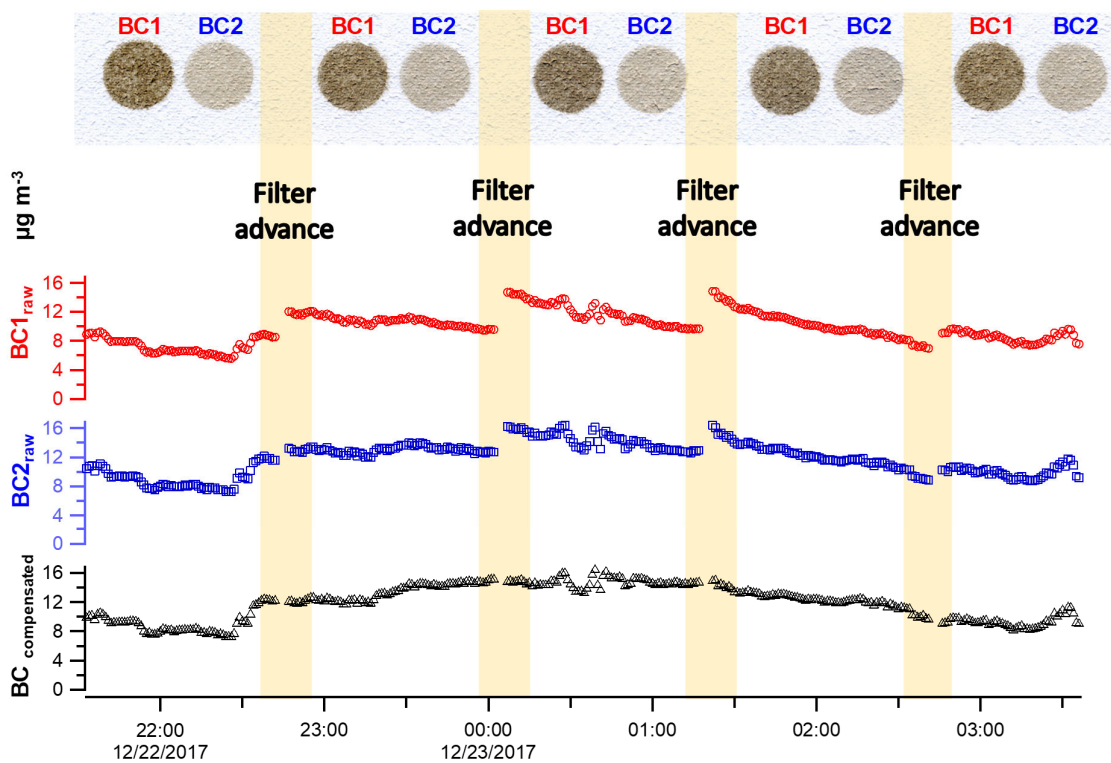


Figure S2. Example of dual-spot data correction. The photo in the upper panel shows the actual appearance of aerosol-laden filter tape used by the AE33 aethalometer. Two spots were used for sample collection during each sampling cycle. The BC1 spot was sampled with a higher flow rate, thus leads to more BC particles deposition, with a darker appearance than the BC2 spot. The panel below shows the raw data from BC1 spot (in red) and from BC2 spot (in blue). The corrected BC is shown in black.

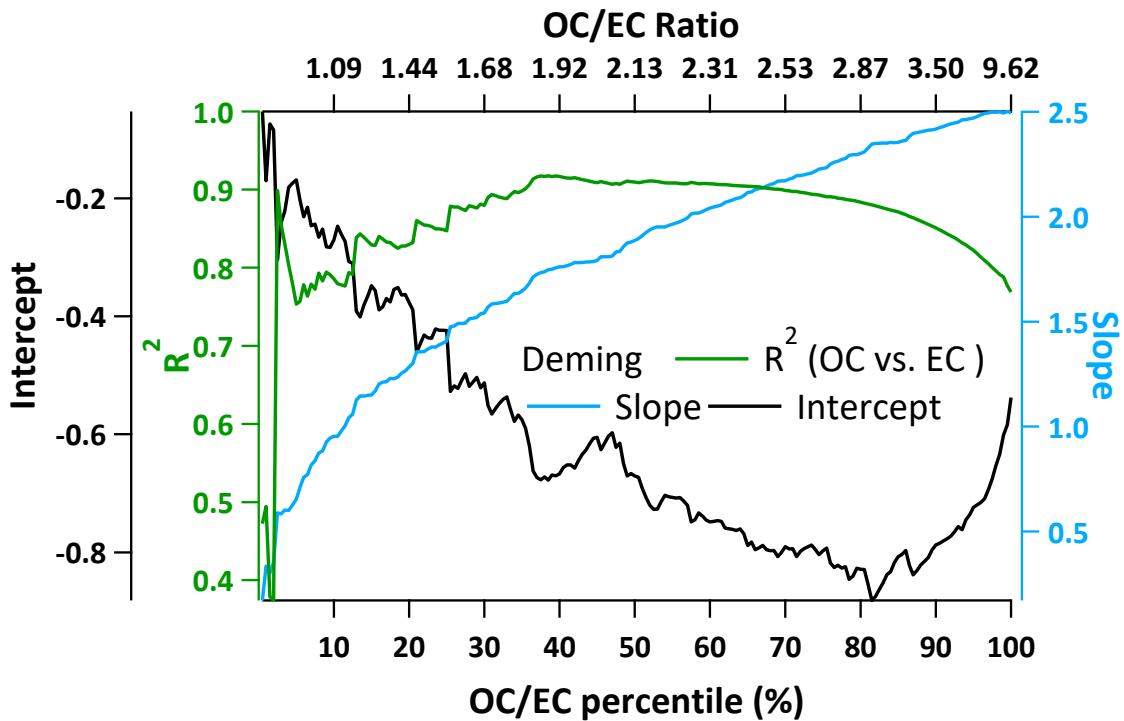


Figure S3. Slope and intercept by orthogonal distance regressions (WODR) as a function of OC/EC percentile from 1 to 100%. The blue curve represents the WODR slope of the corresponding percentile subset. The green curve represents $R^2(OC, EC)$ of the corresponding percentile subset. The black line represents the intercept of the WODR from the corresponding percentile subset (1-100%). The error bars on each curve represents the uncertainty (± 1 S.D.) of slope or intercept.

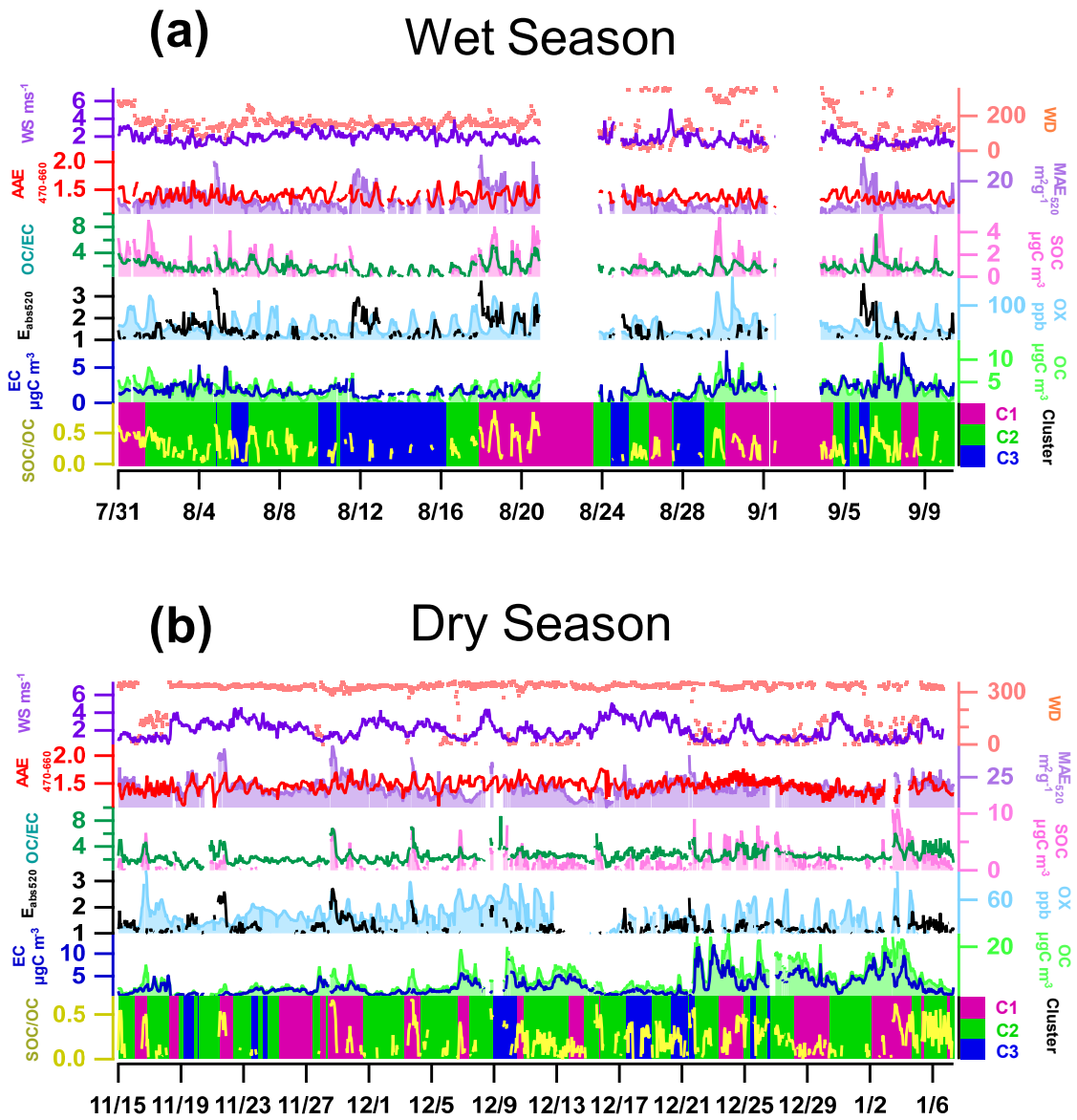


Figure S4. Time series of optical properties and meteorological factors during the two sampling periods. (a) Wet season. (b) Dry season.

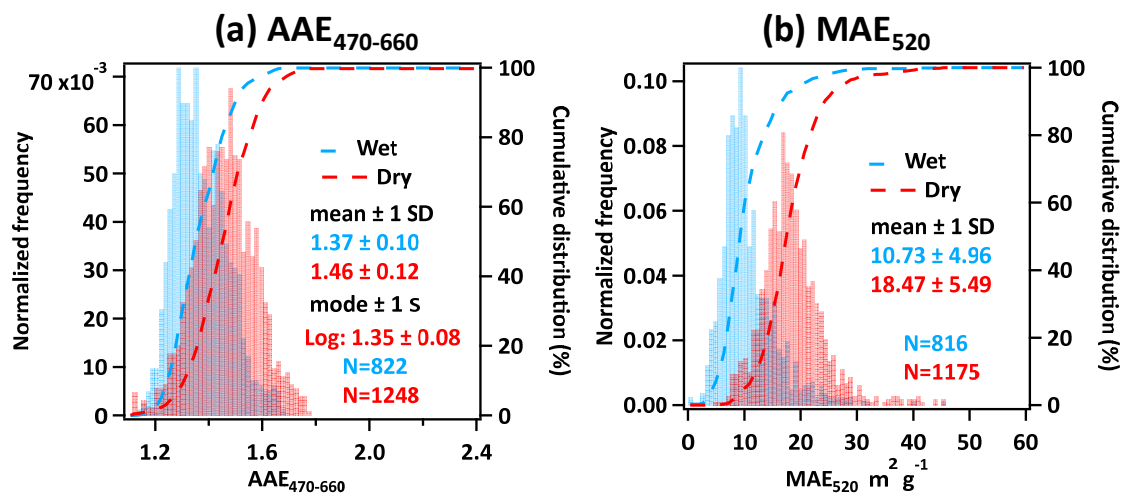


Figure S5. Distribution of AAE₄₇₀₋₆₆₀ and MAE₅₂₀ in wet and dry seasons.

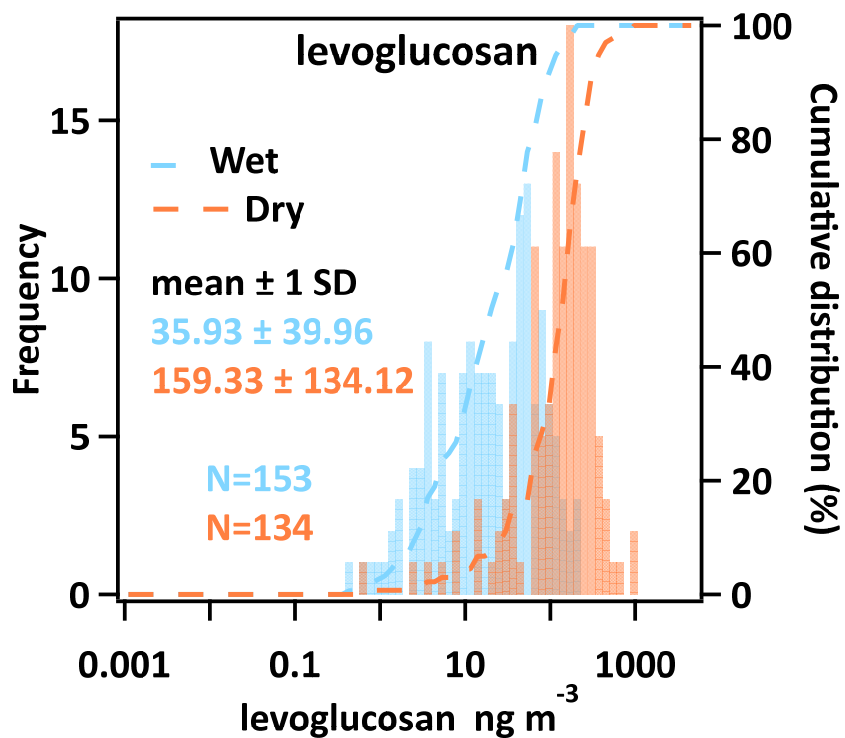


Figure S6. Levoglucosan concentrations measured in Guangzhou during wet and dry season during 2009-2012.

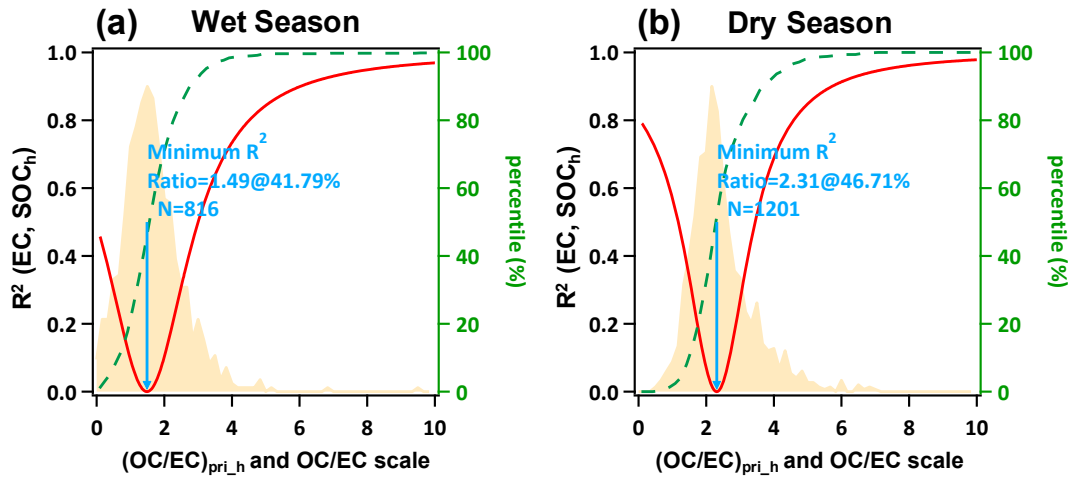


Figure S7. (OC/EC)_{pri} determined by MRS in dry and wet seasons.

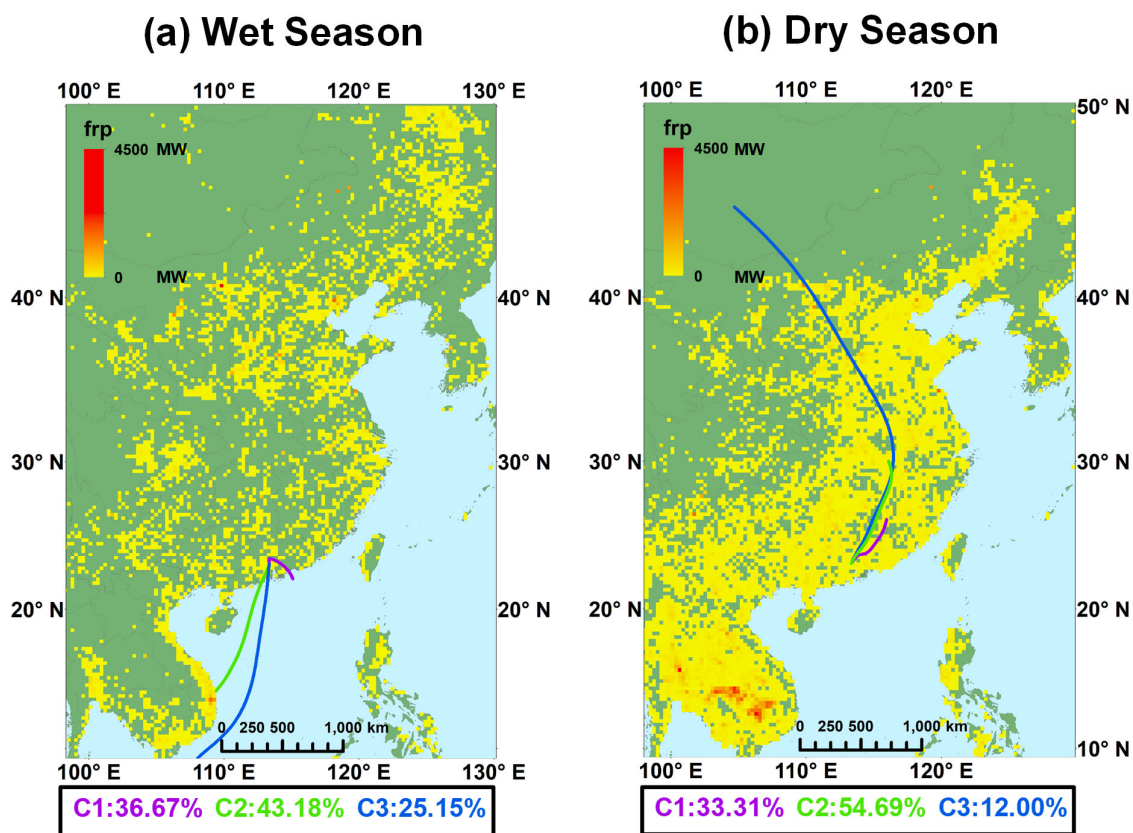


Figure S8. Gridded accumulated fire radiative power (FRP) in MW (megawatts) determined by Visible Infrared Imaging Radiometer Suite (VIIRS) from NASA FIRMS application (<https://firms.modaps.eosdis.nasa.gov/>). Back trajectories clusters analysis results were also plotted overlaid. (a) wet season. (b) dry season.

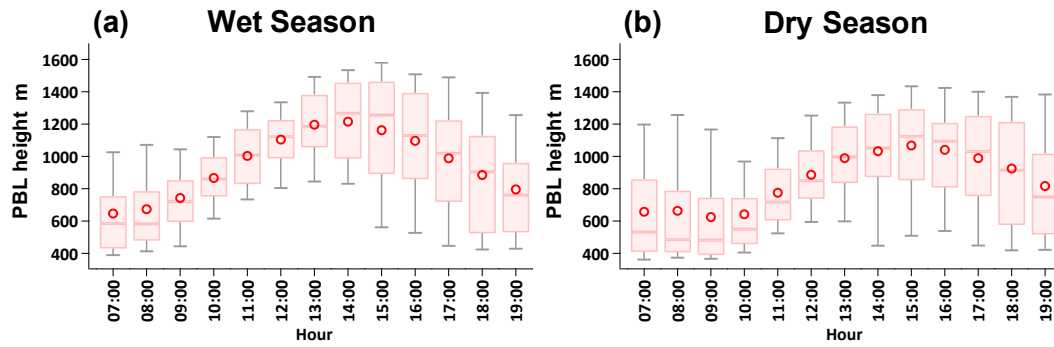


Figure S9. Diurnal patterns of planetary boundary layer height (PBLH) were determined by lidar at the Guangzhou Meteorological Bureau (GMB, 23.00° N, 113.32° E, elevation: 43 m) during September 2013 to November 2014. Red circles represent the hourly averages. The line inside the box indicates the hourly median. Upper and lower boundaries of the box represent the 75th and the 25th percentiles; the whiskers above and below each box represent the 95th and 5th percentiles.

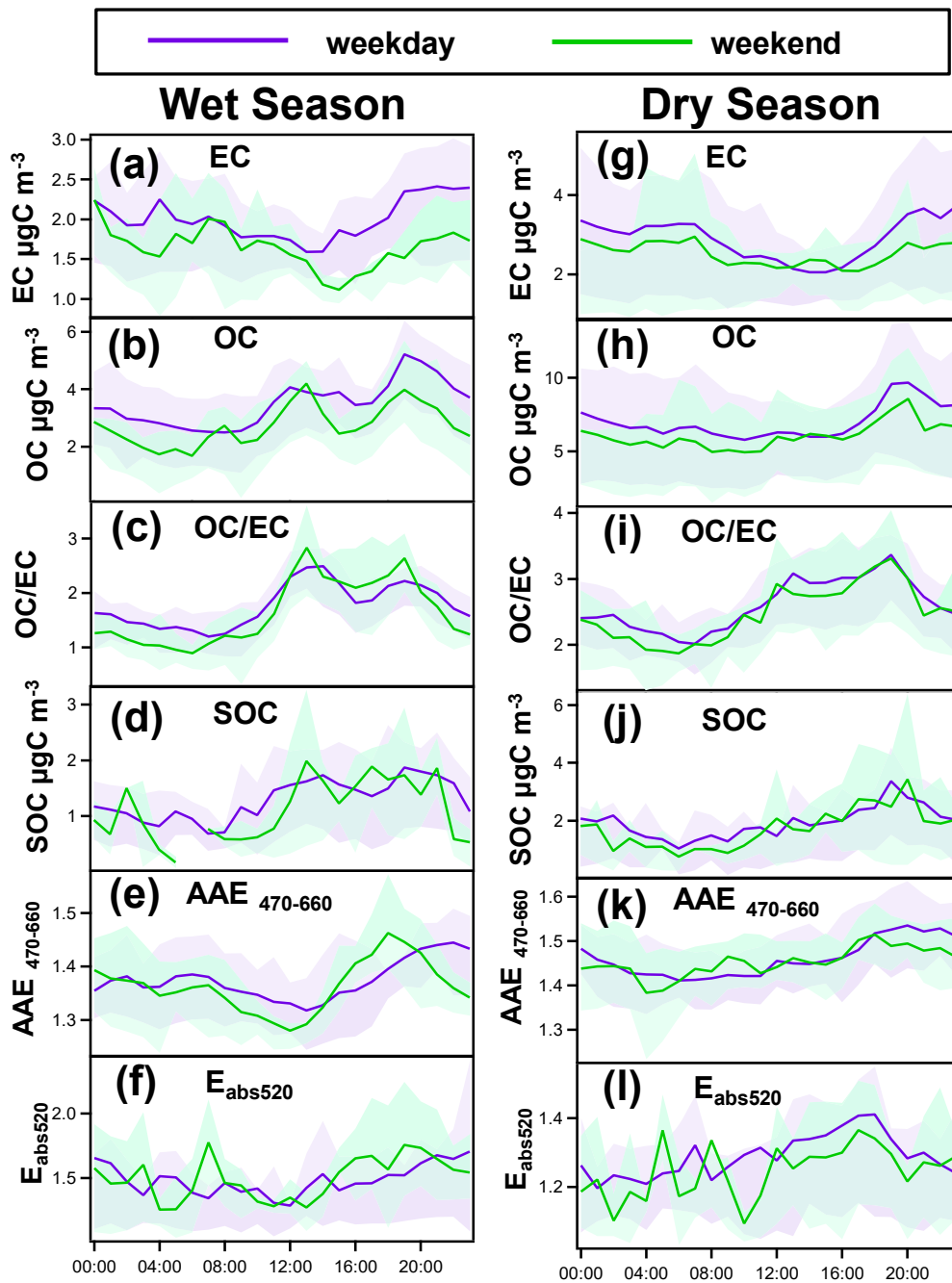


Figure S10. Diurnal pattern of carbonaceous aerosols in wet and dry season segregated into weekdays and weekends.

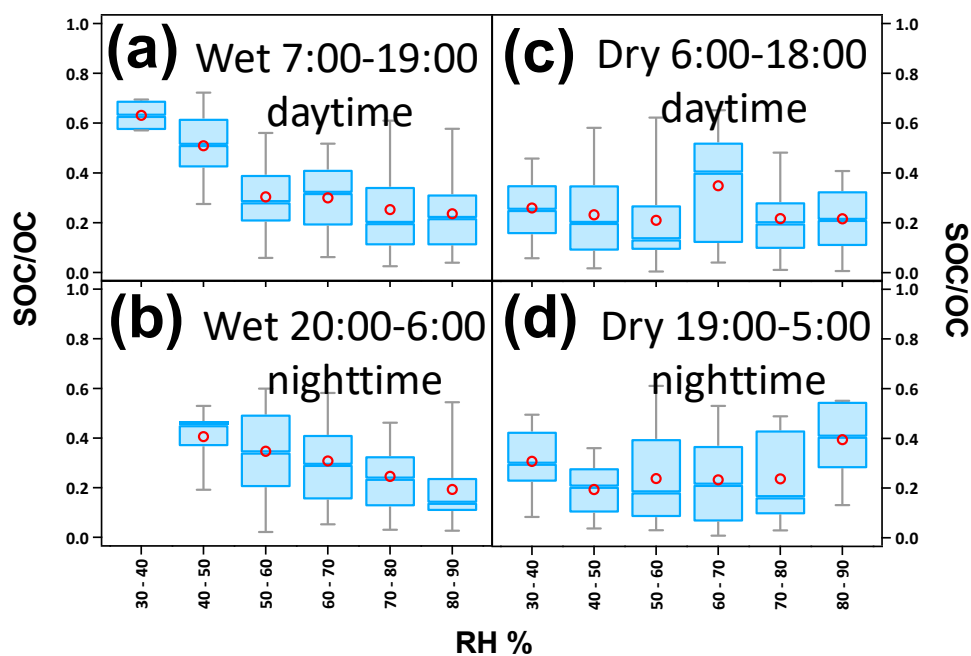


Figure S11. SOC/OC dependency on RH in wet and dry seasons. Red circles represent the average values. The line inside the box indicates the hourly median. Upper and lower boundaries of the box represent the 75th and the 25th percentiles; the whiskers above and below each box represent the 95th and 5th percentiles. (a) SOC/OC dependency on RH in wet season during daytime (7:00 - 19:00). (b) SOC/OC dependency on RH in wet season during nighttime (20:00 - 7:00). (c) same as (a) but for dry season. (d) same as (b) but for dry season.

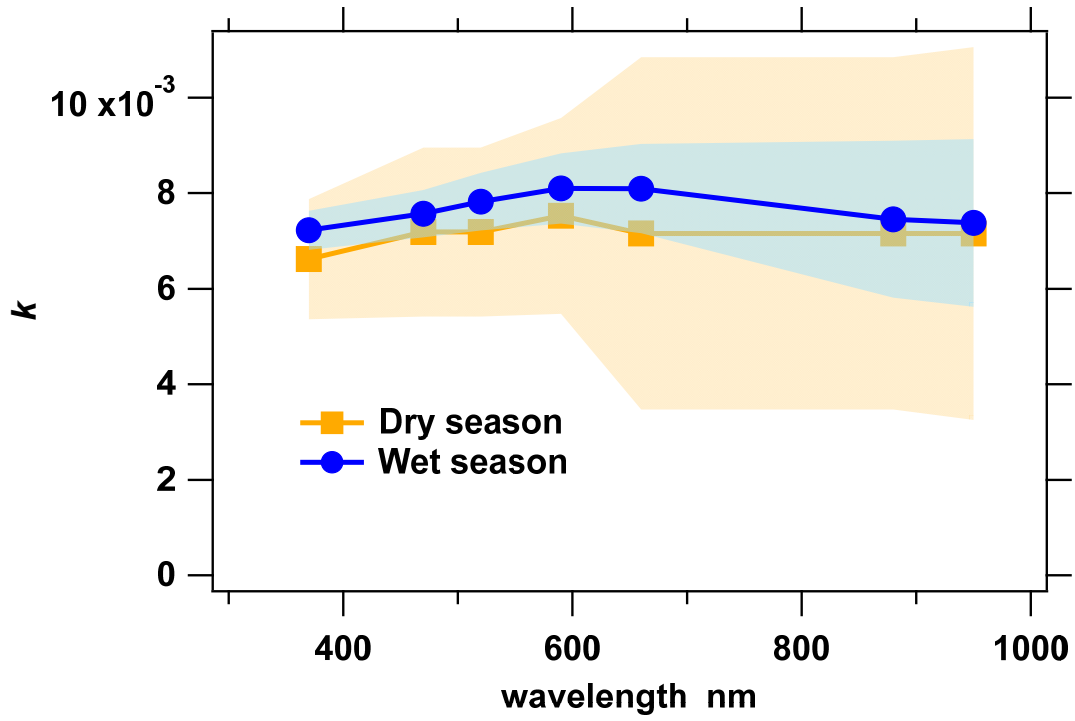


Figure S12. The spectral fingerprints of k between wet and dry seasons. The lines with markers represent mean k values. The shaded areas represent 1 S.D..

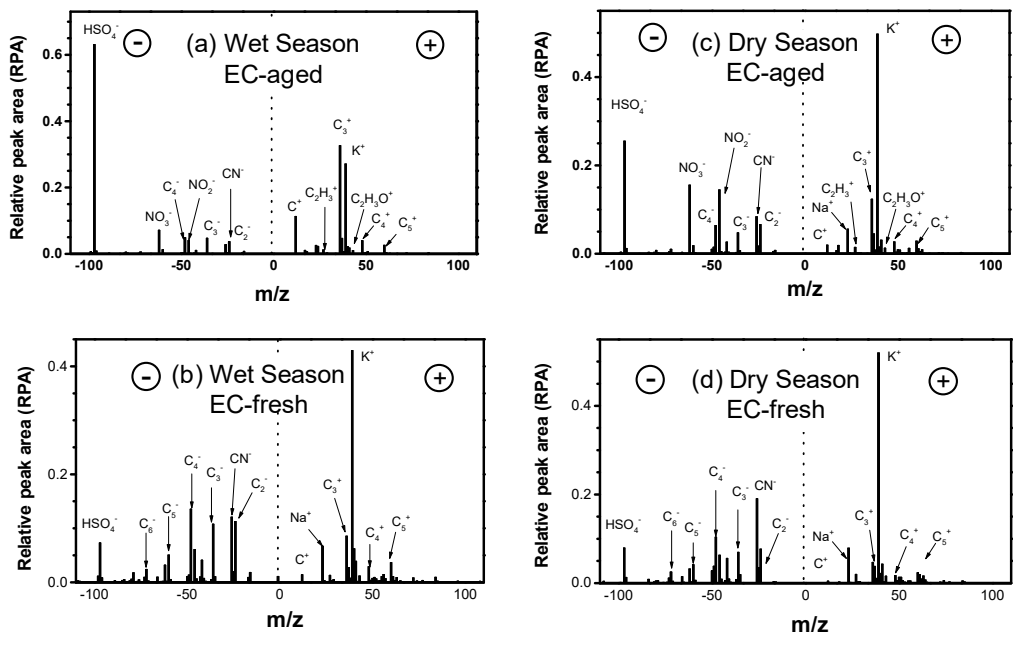


Figure S13. EC-containing particles measured by SPAMS in wet and dry season. Positive and negative mass spectra were shown in the relative peak area (RPA) scale. (a) Average mass spectra of EC-aged particles in wet season. (b) Average mass spectra of EC-fresh particles in wet season. (c) Average mass spectra of EC-aged particles in dry season. (d) Average mass spectra of EC-fresh particles in dry season.

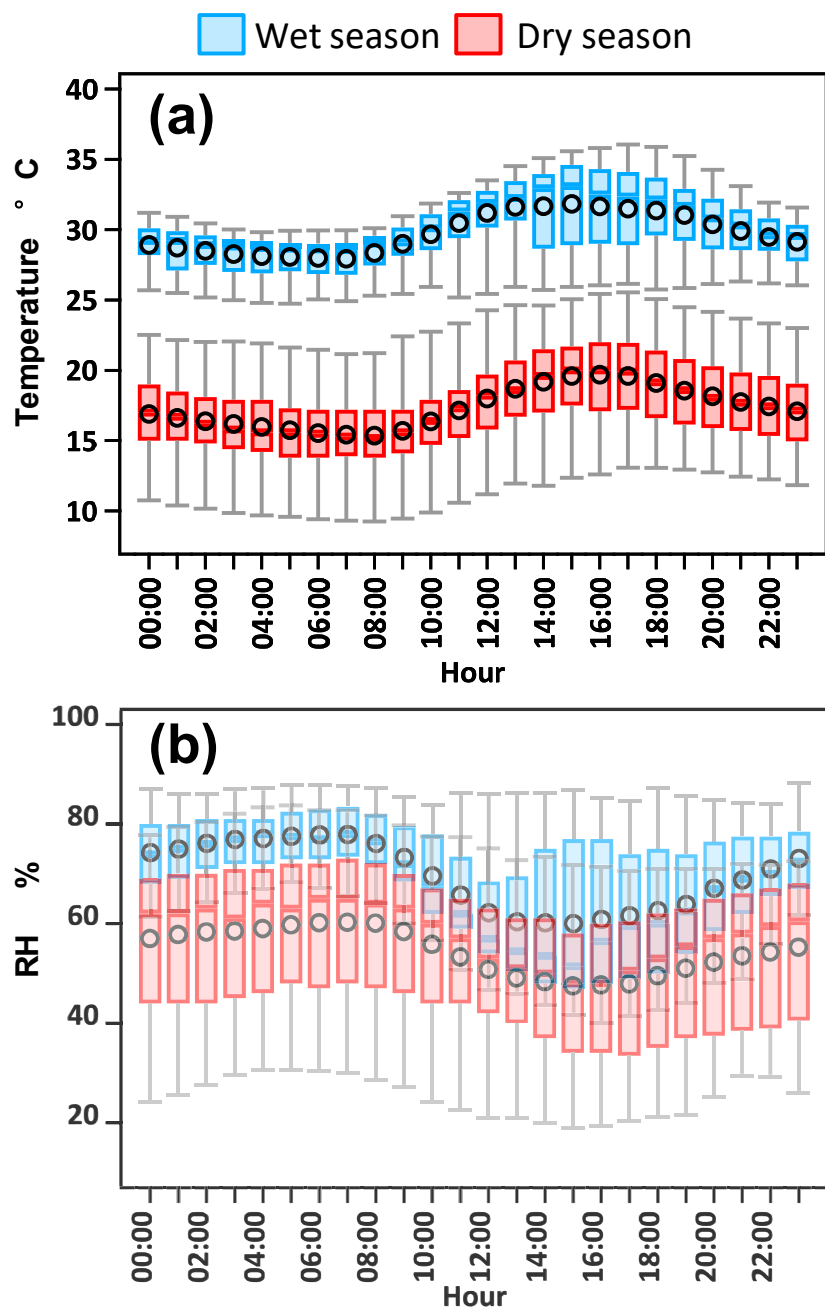
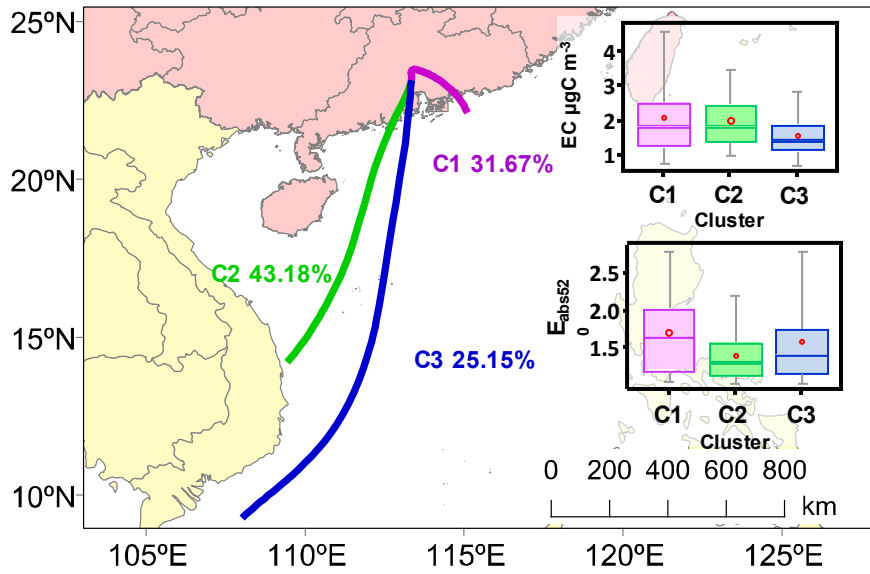


Figure S14. Diurnal variations of temperature and RH during wet and dry season.

(a) Wet Season



(b) Dry Season

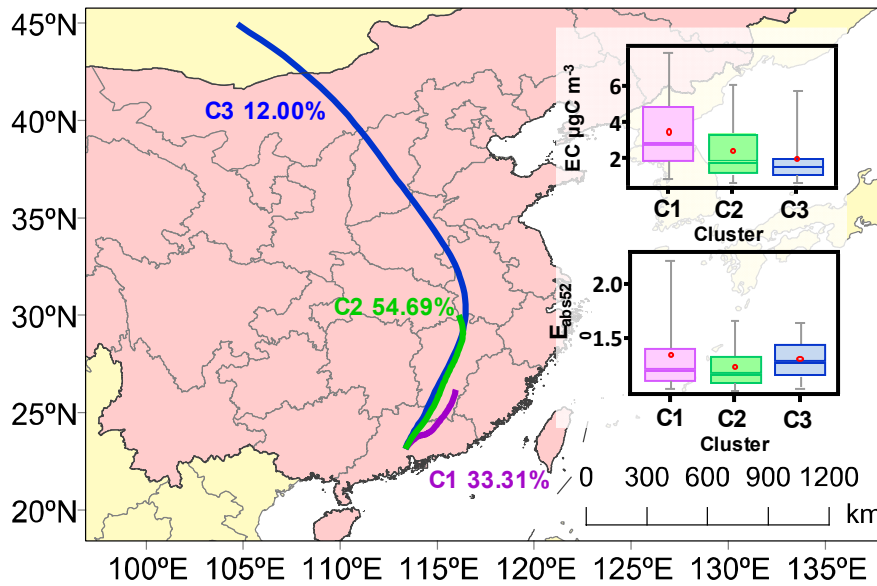


Figure S15. Cluster analysis of back trajectories with EC and E_{abs} . (a) wet season. (b) dry season.

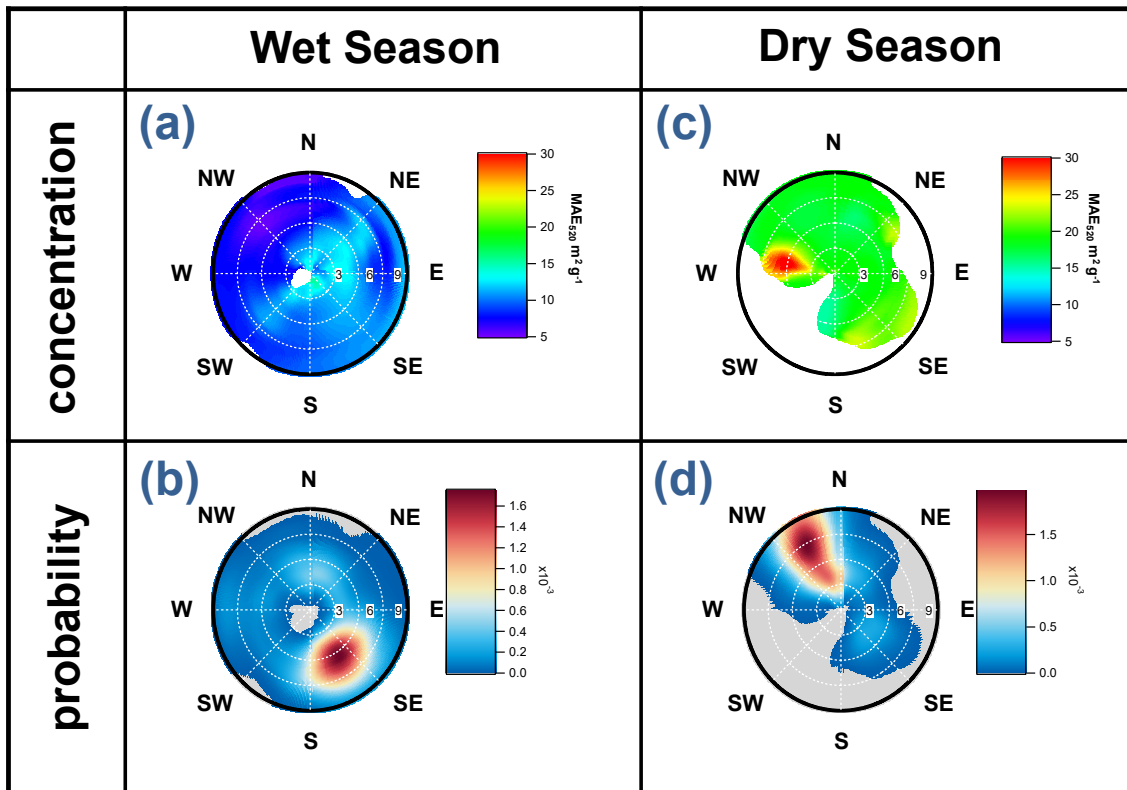


Figure S16. Wind-rose plots that were generated using ZeFir (Petit et al., 2017). The left column shows the distributions of MAE₅₂₀ as a function of wind speed and wind direction, where the color represents the value of MAE₅₂₀ at the corresponding wind speed and wind direction. The right column shows the probability of wind arising from the given wind direction, where the color represents probability.

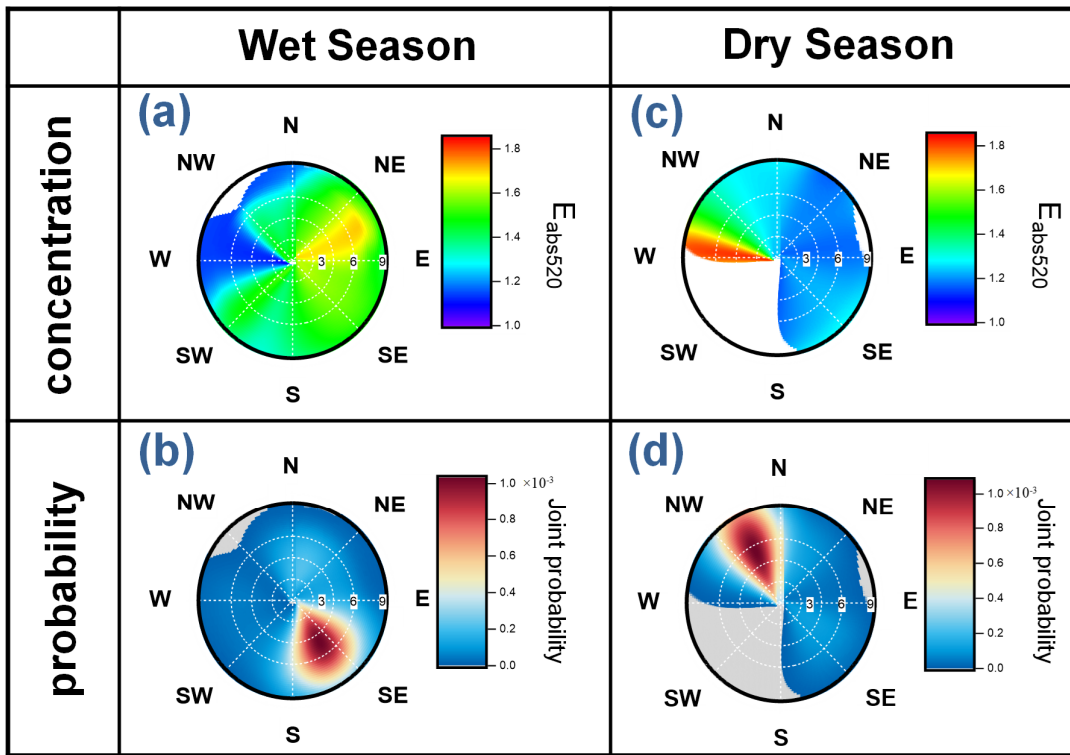


Figure S17. Wind rose plot of Eabs₅₂₀ in wet and dry seasons.